J. Eur. Opt. Society-Rapid Publ. 2024, **20**, 12

https://doi.org/10.1051/jeos/2024011
Available online at: https://jeos.edpsciences.org

Special Issue - Plasmonica 2023
Antonino Foti and Attilio Zilli (Guest editors)

Journal of the European Optical Society-Rapid Publications

RESEARCH ARTICLE

OPEN ACCESS

Towards the epitaxial growth of Au thin films on MgO substrates for plasmonic applications

Michele Celebrano[1], Matteo Savoini[2], Paolo Biagioni[1], Giuseppe Della Valle[1], Giovanni Pellegrini[3], Matteo Cantoni[1], Christian Rinaldi[1], Andrea Cattoni[1], Daniela Petti[1], Riccardo Bertacco[1], Lamberto Duò[1], and Marco Finazzi[1,*]

[1] Dipartimento di Fisica, Politecnico di Milano, Piazza Leonardo da Vinci 32, 20133, Milano, Italy
[2] Institute for Quantum Electronics, ETH Zürich, 8093, Zürich, Switzerland
[3] Department of Physics, University of Pavia, via Bassi 6, 27100, Pavia, Italy

Received 31 January 2024 / Accepted 16 March 2024

Abstract. Surface Plasmon Polaritons (SPPs) in Au thin films are nowadays intensively exploited for sensing applications that leverage the strong optical field confinement at the metal/dielectric interface and the easy functionalization of the Au surface. Moreover, Au thin films represent one of the common starting points for the top-down nanofabrication of plasmonic nanostructures supporting localized resonances. In this framework, strategies for the growth of high-quality Au films on transparent substrates are crucial and not yet fully established. In this study, we exploit MgO(001) substrates for the growth of thin (about 45 nm) Au films, also including an additional buffer layer of Fe. We successfully demonstrate Au samples with reduced roughness and presenting Low-Energy Electron Diffraction (LEED) features, indicating a high degree of crystalline ordering. This is supported by the experimental evidence of an increased (by almost a factor of 3) propagation length compared to a reference Au sample grown on standard glass slides, which is however still significantly lower than the one expected from first principles.

Keywords: Surface plasmon polaritons, Gold, Single crystals.

1 Introduction

Plasmonics investigates the properties of Surface Plasmon Polaritons (SPPs) [1, 2], which are coherent collective electron oscillations travelling together with an electromagnetic wave along the interface between a metal (e.g., Au, Ag) and a dielectric (e.g., glass, air). These surface plasmons can give rise to a wide array of remarkable optical phenomena, such as subwavelength confinement of light and enhanced light-matter interactions, offering the possibility to manipulate electromagnetic fields at the nanoscale. More specifically, by an appropriate choice of geometry and materials, one can tune the plasmonic resonances of nanostructures, enabling the possibility to engineer systems with tailored optical behaviors. These resonances, which can manifest either as surface plasmon resonances at extended metal/dielectric interfaces or as localized plasmon resonances in nanostructures, have found extensive application in a diverse range of fields, including sensing, imaging, energy harvesting, nanophotonics, and data communication [3–5].

Relevant parameters that ultimately define the performance of plasmonic assets consist in field enhancement, spectral selectivity, and SPP propagation length, which are in turn strongly affected by losses [2, 6]. The plasmon energy is in fact lost through different mechanisms, such as absorption, scattering by defects, and radiation leakage, the latter also present in smooth single-crystalline films. Understanding and managing these losses is pivotal in harnessing the full potential of plasmonic technologies.

At planar metal/dielectric interfaces, propagation of SPPs is characterized by a propagation length Λ, which, for a flat and thick film, is mainly determined by Ohmic losses in the metal. Other losses can be due to scattering from surface roughness, grain boundaries, and defects [7, 8]. A further channel is present only for thin films, namely radiation leakage at a second metal/dielectric interface [2, 9].

The propagation length of plasmon polaritons has been characterized on both polycrystalline [10] and single-crystal [10, 11] Au surfaces. In single crystalline thick gold flakes, the SPP propagation length Λ has been found to be as long as about 100 μm for an SPP energy of 1.55 eV and to rapidly decrease to about 1 μm at 2.33 eV, as a consequence

* Corresponding author: marco.finazzi@polimi.it

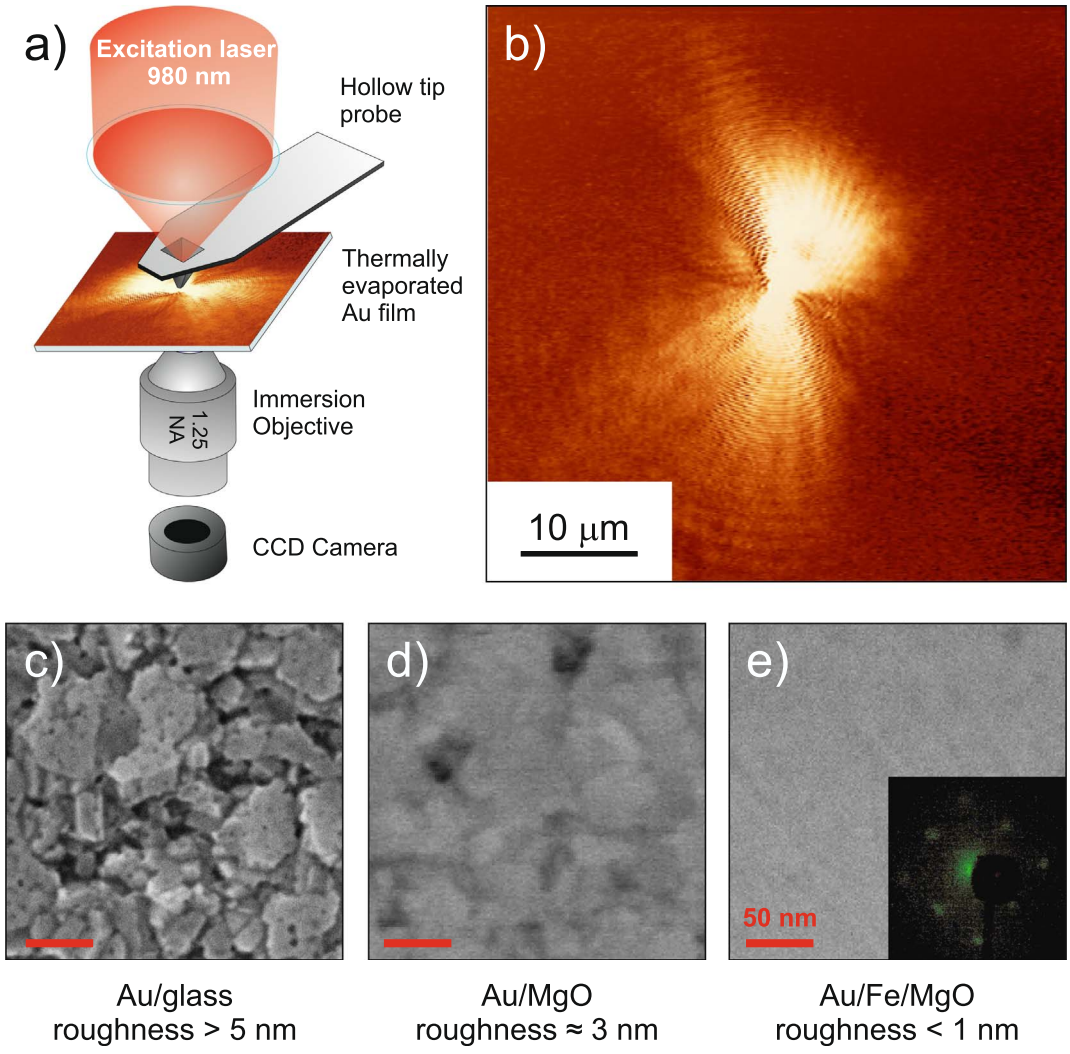

Fig. 1. a) Experimental setup: an SPP wave is launched by a hollow tip for near-field scanning optical microscopy in contact with the gold film. SPP propagation is imaged by collecting the light leaked into the substrate with a CCD camera placed in the focal plane of an oil immersion microscope objective (numerical aperture NA = 1.25). b) Example of an image collected by our experimental setup on the Au/Fe/MgO(001) sample. c–e) Scanning electron microscope images collected on Au/glass, Au/MgO(001), Au/Fe/MgO(001), respectively. Inset: LEED pattern collected on the Au/Fe/MgO(001) sample.

of the rapid increase in the Au resistivity with increasing SPP frequency [11]. The propagation length is found to be strongly damped in polycrystalline samples because of the scattering losses due to the surface roughness and crystal grain boundaries [10]. In practice, so far, single-crystal Au has been mainly studied in bulk (mm-thick) samples [10] and in chemically grown flakes [11], with the relevant exception of the demonstration of high-quality epitaxial thin films on mica substrates [12], which however suffer from a strong birefringence. Another advantage of single crystal Au films consists in the precise control over nanopatterning processes such as electron beam lithography or nanoimprint lithography, enabling the fabrication of high-definition ultrasmooth gold nanostructures with superior optical properties and reproducible nano-sized features over micrometre-length scales [13, 14].

2 Sample preparation and experimental setup

In this work we investigate a possible route to achieve high-quality (possibly single-crystalline) Au thin films by standard Molecular Beam Epitaxy (MBE) on transparent substrates and we experimentally probe the propagation length of SPPs in films characterized by different crystalline and morphological qualities. Surface plasmons are launched by retro-illuminating a hollow tip for near-field scanning optical microscopy in contact with the gold film, similarly to what reported in reference [15]. In this way, SPPs are excited thanks to the large wavevectors associated with the tail of the evanescent field emerging from the subwavelength aperture (diameter ≈ 100 nm). SPP propagation is then imaged at room temperature onto a CCD camera by collecting the light leaked into the transparent substrate

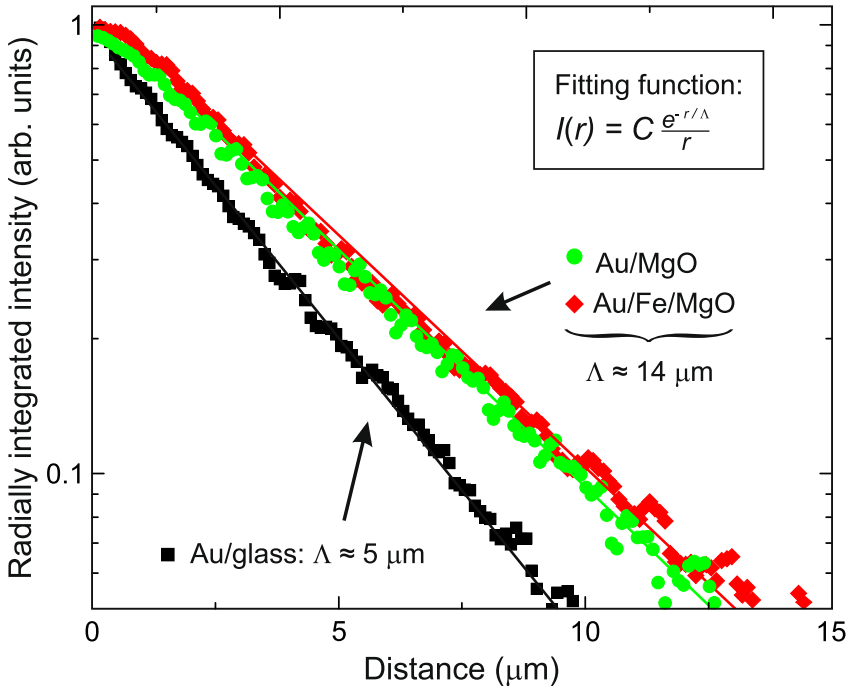

Fig. 2. Normalized radially integrated intensity of the light irradiated by the SPP wave as a function of the distance r from the tip apex. The values of the propagation length Λ obtained by interpolating the data with the function $I(r) = Ce^{-r/\Lambda}$ are reported for all the three investigated samples. The wavelength of light illuminating the tip is $\lambda = 980$ nm, corresponding to a plasmon energy of 1.26 eV.

with an oil immersion microscope objective, characterized by a numerical aperture equal to 1.25 (see Fig. 1a). A typical image measured by the camera is shown in Figure 1b. Extended lobes are seen to protrude from the central position where the tip is located and are visible only when the tip is in contact or next to contact with the Au film. Such lobes are characteristic of a two-dimensional dipole radiation pattern aligned with the linear polarization of the light illuminating the tip aperture [15]. Their shape is however uneven, which we attribute to the irregularities of the contact area between the rim of the tip aperture and the gold film. The concentric rings that can be viewed in Figure 1b are attributed to interference between the radiation leaked from the SPP wave and the light coming directly from the tip aperture, which is a common observation when near-field microscopy is used to image evanescent waves [16].

Gold films with a thickness of 45 ± 5 nm were deposited by MBE onto different substrates by evaporating pure (99.99%) gold pellets by using a Knudsen cell (base pressure during deposition lower than 10^{-9} mbar). The selected substrates were either fused-silica cover-slips or MgO(001) single crystals, the latter characterized by large (hundreds of nanometers wide) atomically-flat terraces. All substrates have been previously cleaned by sonication in isopropanol and then in deionized water. The deposition on MgO(001) crystals was always performed after the homoepitaxial growth of 10 nm of MgO at room temperature, with a rate of about 0.1 nm/min, followed by an annealing at 300 °C for 20 min, in order to create the best surface conditions for the following steps. Au was then either grown directly on MgO or after the evaporation of a 10 nm-thick Fe buffer at a rate of about 0.2 nm/min with the substrate kept at room temperature. The sample was then annealed at 500 °C for 20 min and subsequently flashed at 620 °C [17]. No post-growth annealing was performed on the Au/glass sample since it is well-known that a high-temperature annealing promotes the enucleation of islands, being the surface tension of silica much smaller than the one of the Au film ($\gamma_{\text{silica}} \approx 260$ erg/cm^2 *vs.* $\gamma_{\text{Au}} \approx 750$ erg/cm^2). Au films were deposited with very slow rates (0.1 and 0.5 nm/min) to favour a layer-by-layer growth. Because both rates gave the same structural quality, as checked by Low-Energy Electron Diffraction (LEED) (see Sect. 3), we eventually choose to deposit Au at the faster rate (0.5 nm/min) to reduce the deposition time and, consequently, film contamination (*in-situ* X-ray Photoemission Spectroscopy showed C and O contents below the detection limit). The substrate temperature was chosen to be 120 ± 5 °C because lower temperatures did not show any visible LEED pattern. In the case of the Au/MgO sample, a post-growth annealing at 320 °C for 20 min was performed to improve the film quality, while for the Au/Fe/MgO heterostructure, a post annealing showed no effect. While in the first case (Au/MgO) the quality of the Au film is known to be characterized by the facile nucleation of Au nanoparticles [18] and to be highly sensitive to the carbon content of the substrate [19], the use of an intermediate Fe buffer layer in the Au/Fe/MgO sample has been already shown to improve the crystal quality of the film [20]. A smeared low energy electron diffraction pattern

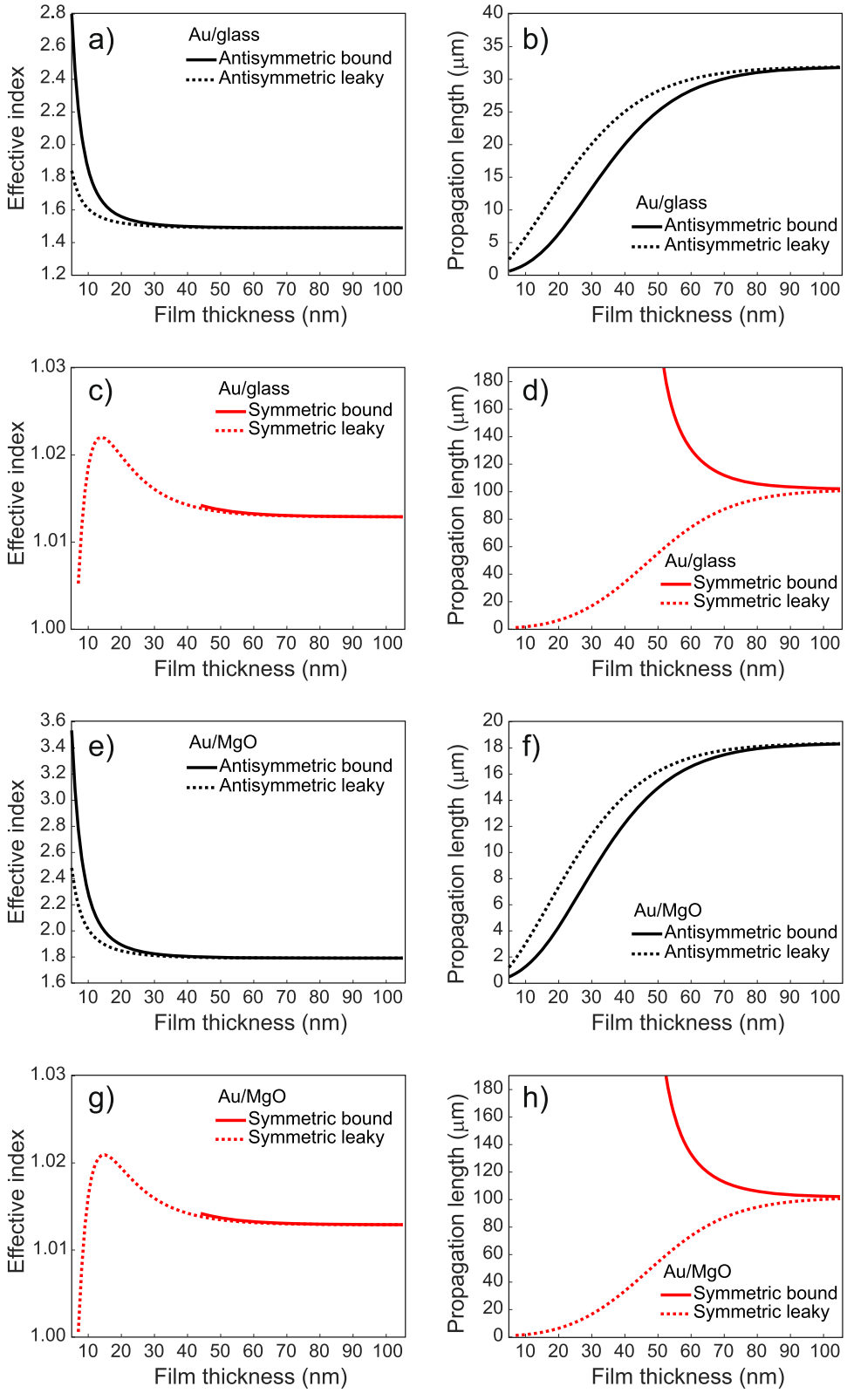

Fig. 3. Analytical results, following reference [6], for the effective index (i.e., the ratio between the free-space and the SPP wavelengths) and the propagation length ($1/e$ attenuation of the SPP intensity) of SPPs propagating in Au thin films on glass (panels a–d) or MgO (e–h). Red lines represent symmetric-like modes, black lines represent antisymmetric-like modes, solid lines refer to bound modes, dotted lines refer to leaky modes.

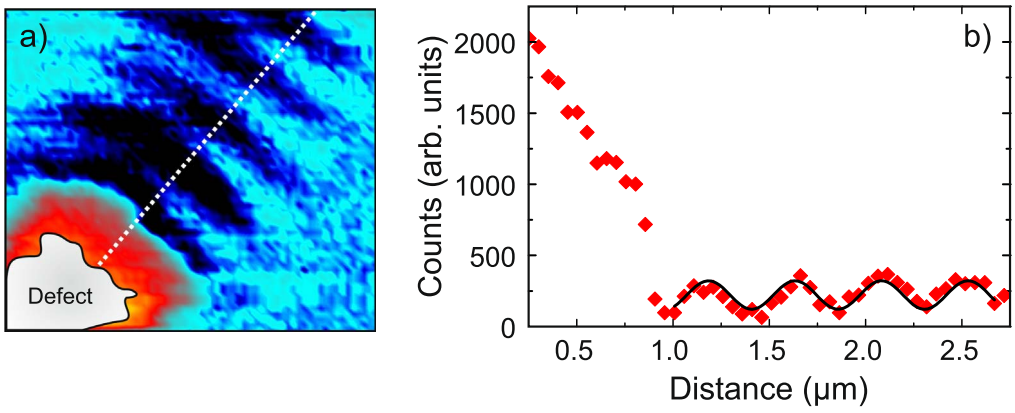

Fig. 4. a) Light collected by the CCD camera showing a stationary wave produced by the interference between the SPP wave excited by the tip (located above the top right corner of the image) and the one back reflected by a large defect on the surface of the Au/Fe/MgO(001) sample. b) Intensity profile (dots) and sinusoidal fitting (line) along the dashed line shown in panel a. From the period of the stationary wave, we obtain that a SPP with wavelength $\lambda_{SPP} = 896 \pm 1.5$ nm is excited by light impinging on the tip with $\lambda_{exc} = 880$ nm.

superimposed on an intense diffused background (see inset in Fig. 1e) is visible for Au/Fe/MgO, after a subsequent post-growth annealing at 390 °C, demonstrating that the insertion of the Fe buffer is indeed effective in improving the crystal quality of the gold layer. A smooth LEED pattern, with a very small contrast compared to the background, was also noticed on a Au/MgO sample with Au thickness of 10 nm. This denotes even in that case some trace of crystal order, which disappears at larger thicknesses. We are not in the position to assess whether such a post-growth annealing also determined interdiffusion between the Fe and the Au layers.

Scanning electron microscope images collected from the three samples are reported in Figures 1c–1e, which show the different morphology of the films. The root-mean square surface roughness was also characterized by atomic-force microscopy to be more than 5 nm, about 3 nm, and less than 1 nm for the Au/glass, Au/MgO, and Au/Fe/MgO samples, respectively.

3 Results and discussion

The normalized radially integrated intensity $I(r)$ of the light radiated by the SPP wave and collected by the camera is shown in Figure 2 for the three investigated samples as a function of the distance r from the tip apex. The three curves can be fitted with an exponential function of the form $I(r) = Ce^{-r/\Lambda}$, where C is a normalization constant and Λ is the SPP propagation length. The wavelength of the light illuminating the tip is $\lambda = 980$ nm, corresponding to a plasmon energy of 1.26 eV. As one can immediately notice, improving the morphology of the Au layer from Au/glass to both Au/MgO(001) and Au/Fe/MgO(001) results in a larger SPP propagation length. However, the additional improvement in the crystalline quality of the Au film achieved through the incorporation of the Fe buffer does not lead to an enhancement in the propagation length.

The value of Λ measured in our thin films is considerably smaller than the one reported for thick Au single crystals, which is about 100 μm for SPP waves excited by light with wavelength $\lambda = 800$ nm (plasmon energy = 1.55 eV) [11]. This observation may not come as a surprise, considering that a smaller propagation length for our samples is to be expected because of the larger radiation losses. As already discussed in the literature [9], the dispersion relations for waves guided by thin, lossy metal films on a substrate include two radiative (leaky) and two nonradiative (bound) modes. The solutions to the analytical problem for the Au/glass and Au/MgO systems can be computed numerically to extract the expected effective index and propagation length following reference [9], as plotted in Figure 3 (Au/Fe/MgO is not shown since the plasmon propagation length estimated for sample is not significantly affected by the extra Ohmic losses, which are negligible with respect to those due to radiation leakage). Leaky and bound modes can be further classified based on their symmetric-like or antisymmetric-like character, which is reminiscent of the symmetric (long-range) and antisymmetric (short-range) SPPs supported by a thin Au film in a symmetric environment [2].

With our experimental configuration, we expect to observe the radiation and decay of the symmetric leaky mode (dashed red lines in Fig. 3), which radiates into the substrates and is characterized by an effective index very close to 1 (see Figs 3c and 3g). On the contrary, the bound modes are not coupled with far field radiation propagating into the substrate and cannot be detected in our experimental configuration The predicted propagation lengths for such mode on 45-nm-thick Au layers is of the order of 40 μm (see Figs. 3d and 3h) and are very similar for the two considered substrates, meaning that the different propagation lengths that we observe in Figure 2 cannot be attributed to the refractive index of the substrates but are rather due to the different surface roughness and/or crystalline quality. To experimentally confirm that this is indeed

the mode we are observing, we look for a sample position in which a surface defect determines the occurrence of an SPP standing wave, as already done in the literature [15]. Figure 4a shows the stationary wave observed when the tip is positioned close to a large defect on top of the Au surface of the Au/Fe/MgO(001) sample. The stationary wave is produced by the interference between the SPP coming from the tip (which is located outside the image, above the top right corner) and the one reflected back by the defect. The half wavelength of the excited SPP can be determined by measuring the period of the stationary wave. We find an SPP wavelength that is about 1% larger than the free-space wavelength of the excitation laser (Fig. 4b). This corresponds to an effective refractive index of 0.98 ± 0.03, thus confirming that, within the error bars for the calibration of our imaging system, we are indeed observing the symmetric leaky mode, which is characterized by an effective refractive index of about 1.015 for a 40 nm-thick Au film. Note form Figures 4a and 4c that the effective indices of the antisymmetric modes are larger than 1.5, therefore the mode can be assigned without ambiguity.

4 Conclusion

In conclusion, we have investigated the propagation length of SPPs propagating at the air/Au interface of thin gold layers deposited onto different substrates and characterized by different morphological and crystalline qualities. The propagation length measured for Au thin films grown on MgO is almost three times larger compared to that of Au film grown on glass. Nevertheless, while we observed an augmented propagation length for samples with better quality, the propagation length reaches a maximum value notably lower (by almost a factor of 3) than the one anticipated by first principle calculations. It should be noticed that for such calculations we have used refractive index data from reference [21], which refers to a polycrystalline Au sample grown on glass that should represent a more disadvantageous situation compared to our high-quality films, both in terms of surface roughness and grain boundaries. It is also worth noting that the absence of any further improvement in the propagation length for the Au/Fe/MgO sample, despite the improved crystallinity, can hardly be attributed to the presence of the Fe layer, which is not predicted to increase the overall Ohmic losses for the symmetric leaky mode in the investigated wavelength range. The quantitative interpretation of our data, therefore, partially remains an open point that confirms the general difficulty in growing high-quality Au films for plasmonic applications and deserves further future investigations to proceed along the route opened by our approach.

Acknowledgments

The authors would like to thank Bert Hecht for insightful discussion.

Funding

This work was supported by Ministero dell'Università e della Ricerca (2017 MP7F8F, PRIN NOMEN).

Conflict of Interests

The authors declare that they have no competing interests to report.

Author contribution statement

Finazzi conceived the experiment. Celebrano and Savoini performed the experiments and analyzed the data. Biagioni, Della Valle and Pellegrini performed the numerical simulations. Cantoni, Rinaldi, Cantoni, Petti e Bertacco realized the samples, Duò coordinated the team.

Data availability statement

The data associated with this study is available upon request. Please contact the corresponding author to request access to the data.

References

1 Maier S.A., Brongersma M.L., Kik P.G., Meltzer S., Requicha A.A.G., Atwater H.A. (2001) Plasmonics – a route to nanoscale optical devices, *Adv. Mater.* **13**, 1501–1505.
2 Maier S.A. (2007) *Plasmonics: fundamentals and applications*, Springer, New York, NY.
3 Lal S., Link S., Halas N.J. (2007) Nano-optics from sensing to waveguiding, *Nat. Photonics* **1**, 641–648.
4 Anker J.N., Hall W.P., Lyandres O., Shah N.C., Zhao J., Van Duyne R.P. (2008) Biosensing with plasmonic nanosensors, *Nat. Mater.* **7**, 442–453.
5 Schuller J.A., Barnard E.S., Cai W., Chul Jun Y., White J.S., Brongersma M.L. (2010) Plasmonics for extreme light concentration and manipulation, *Nat. Mater.* **9**, 193–204.
6 Boltasseva A., Atwater H.A. (2011) Low-loss plasmonic metamaterials, *Science* **331**, 290–291.
7 Aspnes D.E., Kinsbron E., Bacon D.D. (1980) Optical properties of Au: sample effects, *Phys. Rev. B* **21**, 3290–3300.
8 Mills D.L. (1976) Attenuation of surface polaritons by surface roughness, *Phys. Rev. B* **12**, 5539.
9 Burke J.J., Stegeman G.I., Tamir T. (1986) Surface-polariton-like waves guided by thin, lossy metal films, *Phys. Rev. B* **33**, 5186–5201.
10 Kuttge M., Vesseur E.J.R., Verhoeven J., Lezec H.J., Atwater H.A., Polman A. (2008) Loss mechanisms of surface plasmon polaritons on gold probed by cathodoluminescence imaging spectroscopy, *Appl. Phys. Lett.* **93**, 113110.
11 Lebsir Y., Boroviks S., Thomaschewski M., Bozhevolnyi S.I., Zenin V.A. (2022) Ultimate limit for optical losses in gold, revealed by quantitative near-field microscopy, *Nano Lett.* **22**, 5759–5764.
12 Reddy H., Guler U., Kildishev A.V., Boltasseva A., Shalaev V.M. (2016) Temperature-dependent optical properties of gold thin films, *Opt. Mater. Express* **6**, 2776–2802.
13 Huang J.-S., Callegari V., Geisler P., Brüning C., Kern J., Prangsma J.C., Wu X., Feichtner T., Ziegler J., Weinmann P., Kamp M., Forchel A., Biagioni P., Sennhauser U., Hecht B. (2010) Atomically flat single-crystalline gold nanostructures for plasmonic nanocircuitry, *Nat. Commun.* **1**, 150.
14 Grayli S.V., Zhang X., MacNab F.C., Kamal S., Star D., Leach G.W. (2020) Scalable, green fabrication of single-crystal noble metal films and nanostructures for low-loss nanotechnology applications, *ACS Nano* **14**, 7581.
15 Hecht B., Bielefeldt H., Novotny L., Inouye Y., Pohl D.W. (1996) Local excitation, scattering, and interference of surface plasmons, *Phys. Rev. Lett.* **77**, 1889–1892.
16 Biagioni P., Della Valle G., Ornigotti M., Finazzi M., Duò L., Laporta P., Longhi S. (2008) Experimental demonstration of the optical Zeno effect by scanning tunneling optical microscopy, *Opt Exp.* **16**, 3762–3767.
17 Sicot M., Andrieu S., Tiusan C., Montaigne F., Bertran F. (2006) On the quality of molecular-beam epitaxy grown Fe/MgO and Co/MgO (001) interfaces, *J. Appl. Phys.* **99**, 08D301.

18 Benia H.M., Lin X., Gao H.-J., Nilius N., Freund H.-J. (2007) Nucleation and growth of gold on MgO thin films: a combined STM and luminescence study, *J. Phys. Chem. C* **111**, 10528.
19 Rickart M., Roos B.F.P., Mewes T., Jorzick J., Demokritov S.O., Hillenbrands B. (2001) Morphology of epitaxial metallic layers on MgO substrates: influence of submonolayer carbon contamination, *Surf. Sci.* **495**, 68–76.
20 Etienne P., Massies J., Lequien S., Cabanel R., Petroff F. (1991) Molecular beam epitaxial growth of Cr/Fe, Ag/Fe, Ag/Cr and Ag/Co superlattices on MgO (001) substrates, *J. Crystal Growth* **111**, 1003–1010.
21 Etchegoin P.G., Le Ru E.C., Meyer M. (2006) An analytic model for the optical properties of gold, *J. Chem. Phys.* **125**, 164705 .